

# Reconstructing the orbital history of the Veritas family

K. Tsiganis<sup>a,\*</sup>, Z. Knežević<sup>b</sup>, H. Varvoglis<sup>a</sup>

<sup>a</sup> Section of Astrophysics Astronomy & Mechanics, Department of Physics, University of Thessaloniki, GR-54 124 Thessaloniki, Greece

<sup>b</sup> Astronomical Observatory, Volgina 7, 11160 Belgrade 74, Serbia and Montenegro

Received 13 February 2006; revised 26 September 2006

Available online 15 November 2006

## Abstract

The family of (490) Veritas is a young, dynamically heterogeneous asteroid family, located in the outer main belt. As such, it represents a valuable example for studying the effects of chaotic diffusion on the shape of asteroid families. The Veritas family can be decomposed into several groups, in terms of the principal mechanisms that govern the local dynamics, which are analyzed here. A relatively large spread in proper eccentricity is observed, for the members of two chaotic groups. We show that different types of chaos govern the motion of bodies within each group, depending on the extent of overlap among the components of the corresponding resonant multiplets. In particular, one group appears to be strongly diffusive, while the other is not. Studying the evolution of the diffusive group and applying statistical methods, we estimate the age of the family to be  $\tau = (8.7 \pm 1.7)$  Myr. This value is statistically compatible with that of 8.3 Myr previously derived by Nesvorný et al. [Nesvorný, D., Bottke, W.F., Levison, H.F., Dones, L., 2003. *Astrophys. J.* 591, 486–497], who analyzed the secular evolution of family members on regular orbits. Our methodology, applied here in the case of the Veritas family, can be used to reconstruct the orbital history of other, dynamically complex, asteroid families and derive approximate age estimates for young asteroid families, located in diffusive regions of the main belt. Possible refinements of the method are also discussed.

© 2006 Elsevier Inc. All rights reserved.

**Keywords:** Asteroids, dynamics; Asteroids; Celestial mechanics; Resonances

## 1. Introduction

Asteroid families (Hirayama, 1918) are clusters of asteroids in the space of proper elements. Their members are considered to be fragments of larger parent bodies, presumably disrupted by catastrophic collisions in the past. Their study provides important information on the physics of collisions and the composition and mechanical properties of main-belt asteroids (Paolicchi et al., 2002). Asteroid break-ups are considered to be one of the main sources of interplanetary dust (see, e.g., Wyatt, 2005, and references therein). Young asteroid families in particular, corresponding to recent break-ups, are associated with the prominent IRAS dust bands (Nesvorný et al., 2003). Thus, the chronology of formation and the reconstruction of the evolution of family members can provide important information on the collisional evolution of the asteroid belt and the

effects of dust on the Earth's environment (Dermott et al., 2002; Farley et al., 2006).

Recent results have shown that old asteroid families can be approximately dated, on the basis of the distribution of their family members on the  $(H, a_p)$  plane, where  $H$  the absolute magnitude of a body and  $a_p$  the proper semi-major axis of its orbit. Bodies of diameter  $D < 20$  km (large  $H$ ) undergo significant orbital migration, due to the Yarkovsky effect. The amount of Yarkovsky-induced migration is size-dependent,  $\Delta a \sim D^{-1}$  (Farinella and Vokrouhlický, 1999). Thus, as time progresses, families form a characteristic 'V'-shaped distribution on the  $(H, a_p)$  plane. The age of the family can then be approximately computed, by finding the best-fit solution for the width of the  $(H, a_p)$  distribution of family members over a range of age values, using the theoretically expected  $(H, \Delta a)$  curve for given values of the physical parameters of the bodies (Vokrouhlický et al., 2005).

Finding the age of a family that is younger than  $\sim 10$  Myr is a different issue. The Yarkovsky effect would not have had enough time to produce a robust 'V'-shaped signature. How-

\* Corresponding author.

E-mail address: [tsiganis@astro.auth.gr](mailto:tsiganis@astro.auth.gr) (K. Tsiganis).

ever, if the family is located in a region that is dynamically ‘quiet’ (i.e., no strong resonances around), it can be dated, with the use of a method recently proposed by Nesvorný et al. (2002a). Briefly, this method consists in integrating backwards in time the equations of motion for the family members, until the values of the orientation angles of their perturbed elliptical orbits (the longitude of the node,  $\Omega$ , and the argument of pericenter,  $\omega$ ) converge to those they had at the time of break-up. Using this method, Nesvorný et al. (2002a) calculated the age of the Karin family, which turned out to be  $\sim 5.8$  Myr. Nesvorný et al. (2003) applied the same method to the Veritas family and derived an age estimate of  $\sim 8.3$  Myr. Quite recently, Farley et al. (2006) showed that the formation of the Veritas family at that epoch is consistent with geological data, showing an abrupt increase in the influx of  $^3\text{He}$ -enriched interplanetary dust particles on Earth at around the same time.

The Veritas family is not in a dynamically ‘quiet’ region of the belt. The motion of the largest asteroid in the family, (490) Veritas, as that of many other members is chaotic, due principally to the action of the (5,  $-2$ ,  $-2$ ) Jupiter–Saturn–asteroid three-body mean motion resonance (Nesvorný and Morbidelli, 1998, 1999). The chaotic motion of (490) Veritas was first pointed out by Milani and Farinella (1994), who introduced the concept of ‘chaotic chronology’ of a family. They have shown, by numerical integration, that two large members of the family, (490) Veritas and (3542) Tanjiazhen, escape from the family region within  $\sim 60$  Myr, thus providing an upper bound for the age of the family. Subsequently this result has been checked and verified on a larger sample of family members by Knežević (1999) and Knežević and Pavlović (2002), who proposed a more conservative upper bound to the age of the family of  $\sim 100$  Myr, but pointed out that the true age might be significantly shorter.

The existence of many chaotic bodies is the reason why Nesvorný et al. (2003) used only a sub-group of the Veritas family to apply their method; those that appeared to follow regular orbits. However, this can lead to two different interpretations of the results. Nesvorný et al. (2003) pointed out that the 8.3 Myr estimate can be viewed as being either the age of the whole family or the age of the tight group of bodies on regular orbits around (1086) Nata—the second largest body of the family. Thus, it may in fact represent the age of a secondary break-up, that occurred after the family-forming event. Although this seems highly improbable, additional results on the evolutionary history of the chaotic component of the family are needed, in order to exclude this hypothesis. Conversely, given that the results of Farley et al. (2006) strongly support the break-up of a  $D \geq 150$  km asteroid  $\sim 8.3$  Myr ago in the Veritas family region, one could try to reconcile the results of chaotic chronology with the ones of Nesvorný et al. (2003), in an effort to develop a technique that could be used in dating young asteroid clusters, consisting mostly of chaotic bodies.

The method of ‘chaotic chronology,’ as originally proposed by Milani and Farinella (1994), offers a very rough estimate of the age of the family. However, there is probably more information to be extracted from the distribution of chaotic family members. We know that the shape of asteroid families in

the three-dimensional space of proper elements is changing in time, as a result of the combined action of two phenomena: (a) the Yarkovsky effect, which spreads the family members in  $a_p$ , and (ii) the slow chaotic diffusion generated by high-order mean motion and secular resonances, which modify the proper eccentricity,  $e_p$ , and inclination,  $i_p$  of their members. This has been recently demonstrated for the families of (221) Eos (Vokrouhlický et al., 2005) and (158) Koronis (Bottke et al., 2001), as well as for the short-lived resonant population observed in the 7:3 Kirkwood gap, which is kept in steady state by the continuous flux of bodies from these two families (Tsiganis et al., 2003). If a family is relatively young, as it seems to be the case with the Veritas family, the Yarkovsky-driven migration in semi-major axis ( $\Delta a_Y$ ) of  $D \geq 10$  km bodies typically amounts to a very small fraction of the observed extent of the family, and thus can be safely neglected. Then, the long-term effect of chaotic diffusion alone can be studied. Using statistical methods, instead of studying individual orbits, one can obtain a more reliable and accurate estimate for the age of the chaotic component of the family. This is the line of work we follow here.

The goal of the present study is two-fold: (i) to analyze the long-term dynamics of different ‘groups’ of family members, and (ii) to reconcile the results of chaotic chronology on the age of the family, with those of Nesvorný et al. (2003). If the latter is achieved, then our modified chaotic chronology method could be used to estimate the ages of other small asteroid groupings, residing in diffusive regions of the main belt. In the following section, we briefly describe our methodology. Our results are presented in Section 3. Finally, a brief summary and the conclusions of this work are given in Section 4.

## 2. Methodology and techniques

The first step in our study is to identify the members of the Veritas family. We do so by applying the Hierarchical Clustering Method (HCM, Zappalà et al., 1995)<sup>1</sup> to the catalogue of numbered asteroids, maintained by the *AstDys* service (<http://hamilton.unipi.it/astdys>).

For each family member we computed the value of the Lyapunov time of its orbit,<sup>2</sup>  $T_L$ , by integrating the variational equations for 10 Myr and analyzing the output, according to the method described in Tsiganis et al. (2003). Asteroid orbits with  $T_L < 10^5$  yr are usually found in numerical simulations to be unstable within the age of the Solar System. We note though that there exists also a class of asteroids that follow chaotic orbits with  $T_L \sim 10^4$  yr but have stable proper elements for times comparable to the age of the Solar System. The most famous example is Asteroid (522) Helga, which Milani and Nobili (1992) described as the first example of a peculiar type of motion called *stable chaos*. A similar computation of  $T_L$  was made for a set of 400 fictitious objects, chosen so that they cover the same range

<sup>1</sup> The code of HCM was kindly provided by D. Nesvorný.

<sup>2</sup> The Lyapunov time is the inverse of the Lyapunov characteristic exponent,  $\gamma$ , the mean rate of exponential divergence of initially nearby orbits. When  $\gamma \rightarrow 0$  the orbit is regular, while when  $\gamma > 0$  it is chaotic.

of  $a_p$  values as do the real family members. In particular, all fictitious objects were chosen to have the same initial values of osculating elements as (490) Veritas, except for the semi-major axis, which was chosen between 3.1547 and 3.1747 AU. In this way we can evaluate the degree of stochasticity throughout the considered range of  $a_p$  values, and identify different regions of regular and chaotic motion, in which the real family members reside.

Next, we studied the long-term evolution of the proper orbital elements of the family members for 100 Myr; we recall that this was considered an upper bound for the age of the family, before the results of Nesvorný et al. (2003). In fact two integrations were made: first, all real family members were integrated for 10 Myr and, subsequently, the integration was extended to 100 Myr for a sub-group of  $\sim 100$  representative objects. The equations of motion were integrated by means of the public domain *Orbit 9* software package, also available from the *AstDys* service. The physical model assumed in this study is the one in which the (massless) asteroid is subject to the Newtonian gravitational forces of the Sun and the fully interacting four giant planets (Jupiter, Saturn, Uranus and Neptune). Mean elements were computed on-line, by applying digital filtering. Then, for each object, a time series of proper elements was derived, using the analytical theory of Milani and Knežević (1994). A 100 Myr integration backwards in time was also performed, followed by a computation of the corresponding time series of proper elements, for those members of the family that follow regular orbits.

A resonance can generate chaotic diffusion, which may have appreciable effects even on short time scales. This depends on the magnitude of the coefficients of the Fourier harmonics, corresponding to a given resonant multiplet in the expansion of the Hamiltonian,  $\mathcal{H}$ , and the degree of overlap between them (see Morbidelli, 2002). Using our integrations of resonant family members, we calculated the mean squared displacement,  $\langle(\Delta J_k)^2\rangle$ , of each of the two relevant action variables ( $k = 1, 2$ ), which are related to  $e_p$  and  $i_p$ , respectively ( $J_1 \sim \sqrt{a_p} e_p^2/2$  and  $J_2 \sim \sqrt{a_p} i_p^2/2$ ). The average is taken over the corresponding set of family members. In the framework of a simple diffusion approximation, the mean squared displacement in action grows linearly with time, at a characteristic rate that is called *diffusion coefficient*. The diffusion coefficient in each action,  $\mathcal{D}(J_k)$ , was computed as the least-squares-fit slope of the  $\langle(\Delta J_k)^2\rangle(t)$  curve. These computations are used to assess the long-term effect of different resonant multiplets and estimate the corresponding evolution time scales, through a 2-D discrete random-walk model.

### 3. Results

In this section we first present an overview of the family, projected on two proper elements planes ( $a_p, e_p$ ) and ( $a_p, \sin i_p$ ), and discuss some of the observed features. Then, we present our analysis of the distribution of Lyapunov times, with respect to semi-major axis. We distinguish a number of dynamically different groups and analyze the basic properties of motion within each group. We show that two different types of chaotic dynam-

ics are present, each one pertaining to a distinct chaotic group. Finally, a random-walk model is introduced, describing motion in the diffusive zone, and an estimate of the age of the family is derived, through our statistical method of chaotic chronology.

#### 3.1. Distribution in proper elements space

We applied the HCM algorithm to the catalogue of synthetic proper elements of numbered asteroids.<sup>3</sup> The number of identified family members depends on the value of the assumed velocity cut-off,  $v_c$ , as the latter determines the maximum possible deviation of an asteroid's proper elements, with respect to those of the 'central object.' The number of bodies identified as family members by the HCM algorithm is shown in Fig. 1, as a function of  $v_c$ . Two different 'central objects' were used in the identification algorithm: (i) (490) Veritas, which is located in a strongly diffusive chaotic phase-space region, and (ii) (1086) Nata, which is located in a phase-space region of regular motion. As shown in the figure, for  $v_c \leq 26 \text{ m s}^{-1}$ , no family appears to exist around (490) Veritas. This is not true for the other reference object. This result most likely reflects the fact that (490) Veritas has been substantially displaced from its original location, due to chaotic diffusion. For  $v_c > 26 \text{ m s}^{-1}$  the resulting family is the same, whatever the choice of the central object. For  $v_c = 35 \text{ m s}^{-1}$ , the number of family members is 167, while for  $v_c = 40 \text{ m s}^{-1}$  it is 180. We adopt the latter value of  $v_c$ , in order to be able to compare directly our results with the results of Nesvorný et al. (2003), who used the same value in their analysis.

Fig. 1 also shows the distribution of the Veritas family members on the ( $a_p, e_p$ ) and ( $a_p, \sin i_p$ ) planes. The family members have an intricate distribution in the space of proper elements. In particular, the ( $a_p, e_p$ ) distribution suggests that the family can be decomposed into a number of dynamically distinct groups, arranged along the range of  $a_p$  values spanned by its members. The observed extent of the family is  $\delta a_p \approx 0.02 \text{ AU}$  and 93% of the members have  $H \leq 14$  which, assuming a geometric albedo  $p_v \approx 0.07$  (see Di Martino et al., 1997), translates to diameters  $D \geq 8 \text{ km}$ . The Yarkovsky mean drift rate for  $D = 1 \text{ km}$  bodies is  $\dot{a}_Y = 2.7 \times 10^{-4} \text{ AU/Myr}$ , while for  $D > 1 \text{ km}$  it scales as  $1/D$  (Farinella and Vokrouhlický, 1999; see also Tsiganis et al., 2003). Then, over a  $\Delta t = 10 \text{ Myr}$  time interval and for  $D \geq 8 \text{ km}$ , the total drift for most family members is  $\Delta a_Y \leq 3.4 \times 10^{-4} \text{ AU}$ , i.e., less than 2% of  $\delta a_p$ . Thus, if the family is indeed only  $\sim 10 \text{ Myr}$  old, we can safely neglect the Yarkovsky drift in the analysis that follows.

When inspecting the distribution of Veritas family members, it becomes apparent that bodies around  $a_p = 3.168 \text{ AU}$  (group B) and  $a_p = 3.174 \text{ AU}$  (group A) have a larger spread in  $e_p$ , than the rest of the family. The left-hand side of the family (group  $R_1$ ), composed of bodies on regular orbits in the vicinity of (1086) Nata (Nesvorný et al., 2003), fits well inside the elliptical equivelocity curve<sup>4</sup> superimposed on the plot,

<sup>3</sup> We also applied the HCM algorithm to the catalogue of analytical proper elements and found practically no differences.

<sup>4</sup> Computed using the equations of Gauss (see Morbidelli et al., 1995).

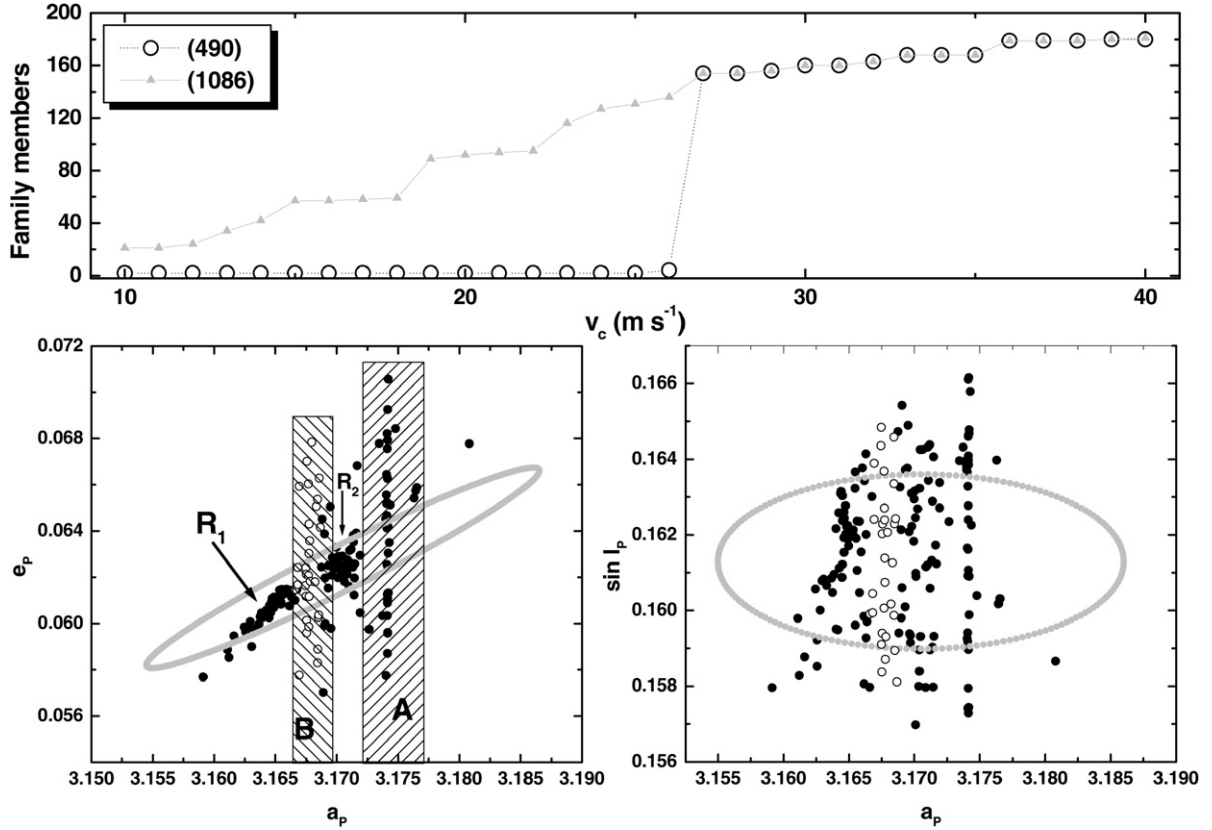


Fig. 1. The Veritas family. (Top) The number of family members as a function of  $v_c$ , using (490) Veritas (open circles) or (1086) Nata (solid triangles) as the ‘central object’ in HCM. The displacement of (490) Veritas, due to chaotic diffusion, results in the absence of other family members in its vicinity for  $v_c \leq 26 \text{ m s}^{-1}$ . (Bottom-left) Distribution of family members in the  $(a_p, e_p)$  plane. The main groups ( $A$ ,  $B$ ,  $R_1$  and  $R_2$ ) are noted. Open circles are used to distinguish the chaotic group- $B$  members. The superimposed ellipse is an equivelocity curve for  $v_c = 40 \text{ m s}^{-1}$  and mean anomaly  $f = 30^\circ$ . This curve is indicative of the initial ejection velocity field. (Bottom-right) the distribution of family members in the  $(a_p, \sin i_p)$  plane. Again an equivelocity curve is superimposed, with  $v_c = 40 \text{ m s}^{-1}$ ,  $f = 30^\circ$  and  $\omega = 150^\circ$ .

while groups  $A$  and  $B$  are cutting through this ellipse, producing two ‘finger-like’ features. Similar, but less pronounced, features are also observed in the  $(a_p, \sin i_p)$  distribution. The remaining component of the family (group  $R_2$ ) is located between the two dispersed groups and has a very small spreading in  $e_p$ , much like the  $R_1$  group. If we assume the borders of the distribution of asteroids in  $(a_p, e_p)$ , immediately after the family-forming break-up, to be roughly described by an equivelocity ellipse similar to the one plotted in Fig. 1, then the initial spread in eccentricity for group- $A$  and group- $B$  objects should have been much smaller than nowadays observed. For what concerns  $\sin i_p$ , the differences in spread between these two groups and the rest of the family are not so pronounced, as indicated by the equivelocity curve that is plotted in the respective diagram. The fact that most family members fit well inside the ellipse suggests that much of the observed spread in  $\sin i_p$  is probably due to a large vertical component of the initial ejection velocity field.

It is known that the ‘finger-like’ features observed as groups  $A$  and  $B$  are associated with the action of three-body mean motion resonances (Nesvorný and Morbidelli, 1998, 1999; Knežević et al., 2002; Nesvorný et al., 2003) among Jupiter, Saturn and the asteroid; hence also the alignment of the resonant asteroids about the same value of  $a_p$  (see Fig. 1), due to

the failure of the standard averaging procedure in the computation of resonant proper elements. Even if this does not affect the present analysis, as a matter of principle one could compute especially adapted proper elements for each resonance (Morbidelli et al., 1995), but then non-resonant and resonant proper elements could not be used at the same time, e.g., for family identification purposes. An analysis of the long-term effects of these resonances is given in the following sections.

### 3.2. The main dynamical groups

We proceed with the analysis of our numerical integrations. In Run I (10 Myr integration) we determined the value of  $T_L$  for every orbit, starting with a population that consisted of the 180 real Veritas family members and 400 fictitious objects, as mentioned in the previous section. In Run II we computed the time evolution of proper elements of the real objects over a 10–100 Myr time interval, as also explained in the previous section.

Fig. 2 shows the results of Run I, i.e.,  $T_L$ , as a function of semi-major axis. In order to be able to superimpose the two populations, we had to circumvent the following problem: all fictitious bodies were regularly spaced in terms of their osculating values of  $a = a_0$  at  $t = 0$ , which is not true for the real

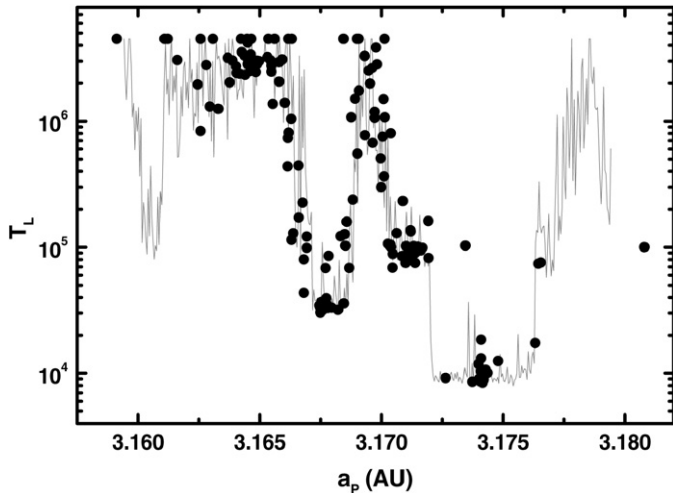


Fig. 2. The Lyapunov time of test particles (grey line) and the real Veritas family members (black dots), as a function of  $a_p$  (see text for details). The superposition of the two groups reveals the dynamical heterogeneity of the family.

objects, while all other elements were equal to the ones of (490) Veritas at the considered epoch. Since all fictitious objects had the same phases, their spacing<sup>5</sup> in osculating  $a_0$  represents their spacing in  $a_p$ . On the other hand,  $a_p$  is known for the real family members. Thus, a superposition of the real objects on the ‘background’  $T_L(a)$  function can be done by adding a small correction term to the  $a_0$  value of each fictitious object. This correction term is equal to  $\delta a = (a_p - a_0)_{490} \approx 0.004$  AU, i.e., the difference between the proper and osculating values of  $a$  for (490) Veritas.

As shown in Fig. 2, there are two broad chaotic bands cutting through the family, characterized by two different values of  $T_L$ : group-A bodies, including (490) Veritas itself, reside in the  $T_L = 10^4$  yr chaotic band (see also Fig. 1) while most group-B bodies (62%) are located in, or close to, the  $T_L = 3 \times 10^4$  yr band. The rest of group-B asteroids, as well as the  $R_2$  bodies, are located between these two main chaotic bands. Chaotic sidebands are also observed on both sides of the  $T_L = 10^4$  yr band. The one on the l.h.s., with  $T_L \sim 10^5$  yr, is more prominent and many  $R_2$  bodies are in fact located therein. We note though that no sizeable region of regular motion appears to exist between the  $T_L = 10^4$  yr chaotic band and the thinner  $T_L \sim 10^5$  yr band; hence the characterization sideband. Finally, two more chaotic bands appear on either edge of the considered  $a_p$  interval. Only one family member can be found in the r.h.s. end of the diagram: Asteroid (37005) 2000TO37, at  $a_p \approx 3.18$  AU.

The  $T_L = 10^4$  yr band is associated with the  $(5, -2, -2)$  Jupiter–Saturn–asteroid mean motion resonance (Nesvorný and Morbidelli, 1998). The  $T_L = 3 \times 10^4$  yr band is associated with the  $(3, 3, -2)$  resonance (Knežević et al., 2002). Asteroid (37005) moves in the vicinity of the  $(7, -7, -2)$  resonance. These two latter resonances arise from frequency combinations of the main  $(5, -2, -2)$  resonance and the  $\sim 2/5$  ‘Great In-

equality’ between Jupiter and Saturn.<sup>6</sup> According to Fig. 2, the  $(3, 3, -2)$  resonance has a width of  $\sim 2 \times 10^{-3}$  AU. This is the same value as the one determined numerically by Nesvorný and Morbidelli (1998), but significantly larger than the one of  $0.13 \times 10^{-3}$  AU, expected by their analytic model (Nesvorný and Morbidelli, 1999). This discrepancy is probably related to the fact that the chaotic zone is produced by the overlapping of many adjacent resonant harmonics while, in the analytic model, the width of a single harmonic is computed, in the pendulum approximation. Finally, Knežević et al. (2002) suggested that the  $T_L = 10^5$  yr sideband is probably due to the  $(8, 1, -4)$  three-body resonance, since at least one  $R_2$  asteroid was found to perform libration in one of the critical arguments of this resonance.

The evolution of the digitally filtered elements of two resonant bodies is shown in Figs. 3 and 4. In Fig. 3 we show the time evolution of the group-A Asteroid (8726). The long-period variations of its filtered  $a$  are well correlated with the variations of the critical argument  $\sigma_{(5,-2,-2)} = 5\lambda_J - 2\lambda_S - 2\lambda - \varpi$  of the  $(5, -2, -2)$  resonance. We remind the reader that irregular transitions of the critical argument from libration to positive or negative circulation strongly suggest that the motion takes place in the stochastic layer of the respective resonance. The long-term effects of this chaotic behavior are examined in the following subsection.

In Fig. 4 we show the time series of semi-major axis and eccentricity of the group-B Asteroid (23433), along with two  $(3, 3, -2)$  critical arguments;  $\sigma_1 = 3\lambda_J + 3\lambda_S - 2\lambda - \varpi_J - 2\varpi_S - \varpi$  and  $\sigma_2 = 3\lambda_J + 3\lambda_S - 2\lambda - 2\varpi_J - 2\varpi$ . The semi-major axis time series is characterized by short-periodic oscillations, superimposed on a ‘proper’- $a$  curve, which itself suffers from long-periodic variations. The ‘proper’- $a$  curve is calculated by applying running-window averaging on the filtered data. The long-periodic variations of this ‘proper’  $a$  are related to the action of the  $(3, 3, -2)$  resonance, whose critical arguments show transitions from libration to circulation on comparable time scales. Typically, more than two (but not many more) arguments show erratic behavior, which explains the chaotic motion of group-B asteroids and suggests that several  $(3, 3, -2)$  harmonics are partially overlapping. The short-periodic oscillations of  $a$  may be related to the effects of the neighboring  $(5, -2, -2)$  resonance (Morbidelli, personal communication). It is clear from Fig. 4 that the amplitude of these oscillations maximizes when the filtered eccentricity is at minimum (vertical grey dashed lines), while it almost vanishes when the eccentricity is at maximum (vertical black dashed lines). Note that  $e$  is maximum when  $\varpi = \varpi_J$ , while it is minimum when  $\varpi = \varpi_J + \pi$ . Thus, when  $e$  is maximum, the perihelia of Jupiter and the asteroid are aligned and the two main harmonics of the  $(5, -2, -2)$  resonance cancel out (see Ta-

<sup>5</sup> Apart from very small variations related to their small differences in  $e_p$  and  $i_p$ .

<sup>6</sup> Note that in Nesvorný et al. (2003) the resonance responsible for the chaotic behavior of group-B bodies was erroneously identified as  $(7, -5, -2)$ , instead of the  $(3, 3, -2)$  one, found by Knežević et al. (2002). The correct identification appears in Nesvorný et al. (2002b).

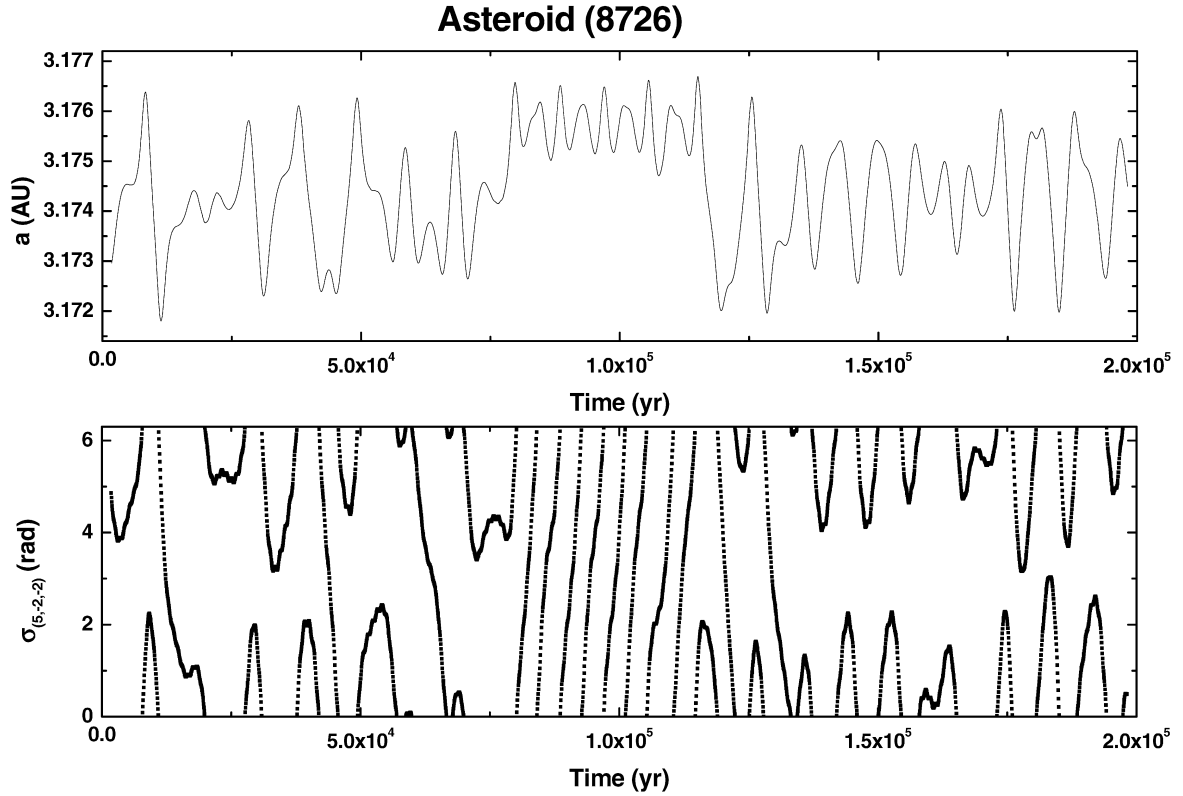


Fig. 3. (Top) Time series of the digitally filtered semi-major axis for the group-A Asteroid (8726). The corresponding critical argument (bottom) is  $\sigma_{(5,-2,-2)}$  (see text). This asteroid spends most of the time performing *libration* around  $a \approx 3.174$  AU. For  $80,000 \leq t \leq 115,000$  yr the asteroid moves near the outer border of the resonance, i.e., it circulates at  $a \approx 3.176$  with  $\dot{\sigma}_{(5,-2,-2)} > 0$ .

ble III in Nesvorný and Morbidelli, 1999). Conversely, when  $e$  is minimum, the perihelia are anti-aligned and the two main  $(5, -2, -2)$  harmonics sum up, giving rise to higher perturbations in  $a$ .

Group  $R_1$  (see Figs. 1 and 2) seems to be composed exclusively of asteroids on regular orbits. This was indeed confirmed by the results of Run II. Their proper elements are stable over a 100 Myr time interval, as was found by our backwards-time integration. A slightly different behavior is observed for the members of the  $R_2$  group, as well as the members of group  $B$  that lie outside the  $(3, 3, -2)$  chaotic band. The nearby resonances induce long-periodic small amplitude perturbations on their orbits. However, these perturbations do not seem to ‘build-up,’ at least within 100 Myr. Thus  $R_2$ , as well as non-chaotic group- $B$  asteroids, have very stable proper elements over a 100 Myr time span. In this respect their long-term behavior is very similar to that of  $R_1$  bodies (see Fig. 5). Note that in the following study of the past evolution of regular family members we will only consider  $R_1$  bodies, since they are less affected by the main resonances.

From the point of view of chaotic chronology of the family, group  $A$  and the chaotic part of group  $B$  are most interesting, since their members have (i) the largest spread in  $e_p$  and (ii) the smallest values of  $T_L$  (most chaotic orbits). Thus, in the following subsection, we focus on the long-term evolution of these two groups.

### 3.3. Diffusive vs non-diffusive chaos

Let us now examine more closely the motion inside the two main chaotic bands. The results of Run II are summarized in Fig. 6. The traces of all chaotic asteroids during the first 10 Myr of their evolution in the space of proper elements are shown as dark-grey dots, while their traces for the whole 100 Myr interval are represented by small light-grey dots. The present-day distribution of family members is plotted for reference (open triangles). The different behavior of the two chaotic groups is evident. Group- $A$  bodies diffuse very efficiently in  $e_p$  and  $\sin i_p$ . During the first 10 Myr they cover a phase-space region that is about twice as big as the initial one, in terms of eccentricity and inclination ( $e_p$  between  $\sim 0.037$  and  $\sim 0.087$  and  $\sin i_p$  between  $\sim 0.155$  and  $\sim 0.175$ ). After 100 Myr the traces of group- $A$  asteroids cover a range of  $e_p$  between zero and 0.1 and  $\sin i_p$  between 0.14 and 0.18 (i.e.,  $\Delta i_p \approx 2^\circ.3$ ). Note though that no object escaped from the  $(5, -2, -2)$  resonance zone, the mean value of  $a_p$  being always close to 3.174 AU.

The behavior of chaotic group- $B$  asteroids is surprisingly simpler than that of group- $A$  asteroids. Their traces practically cover the same region, as the one occupied by their present-day distribution, and no macroscopic diffusion is observed. This may seem strange, given that the two chaotic groups have similar values of  $T_L$ . However, one has to remember that the size of the long-term variations of proper elements is related to the resonance involved and not to the value of  $T_L$ . Several reso-

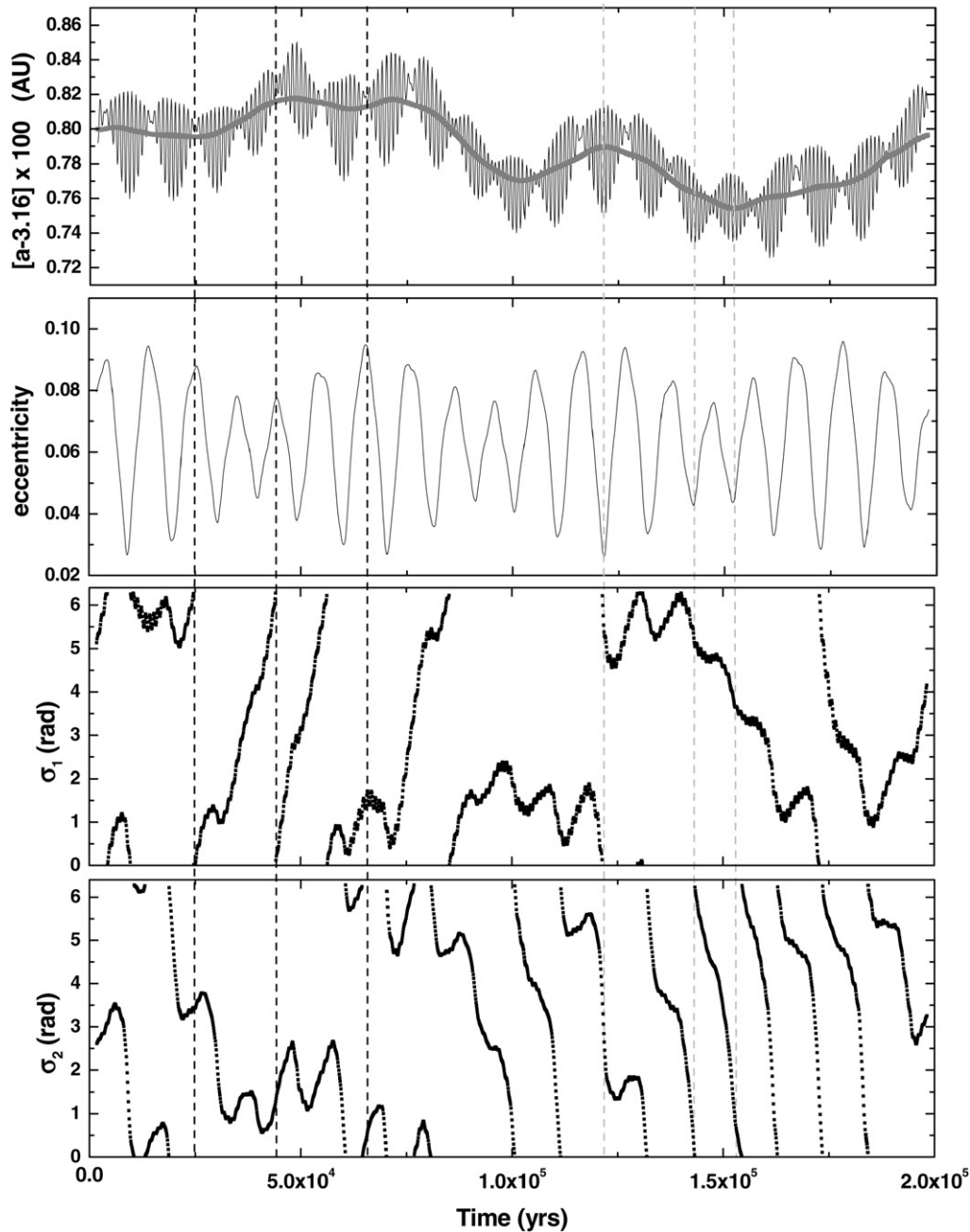


Fig. 4. Time series of the digitally filtered semi-major axis and eccentricity for the group-*B* Asteroid (23433). Two critical arguments of the (3, 3, -2) resonance are also shown (see text for details). The long-term variations of the ‘proper’  $a$  (grey line on top panel) are correlated with transitions of the (3, 3, -2) resonant arguments from libration to circulation.

nances may have similar values of  $T_L$  in their chaotic layers, but very different long-term stability properties, as the existence of stable-chaotic asteroids shows (Milani and Nobili, 1992). The critical parameter for long-term stability is the degree of overlapping between the harmonics of each resonance multiplet. Murray and Holman (1997) have shown that the Lyapunov time in high-order resonances is of the order of the secular precession period,  $2\pi/\dot{\omega}$ , where  $\dot{\omega}$  represents also the distance between the harmonics of a resonant multiplet in frequency space, and is almost constant throughout the observed range of the family. On the other hand, the width of each harmonic in

frequency space depends on the amplitude of the coefficient of the respective term in the Fourier expansion of  $\mathcal{H}$ . Performing an expansion of the three-body disturbing function, Nesvorný and Morbidelli (1999) have shown that the (5, -2, -2) resonance is the strongest three-body resonance in the main belt. In fact its harmonics completely overlap each other, giving rise to a dynamical behavior that is very similar to the one of a slowly modulated pendulum (see also Morbidelli, 2002). This was verified by Knežević et al. (2002), who analyzed the behavior of different critical arguments of this resonance for several group-*A* asteroids.

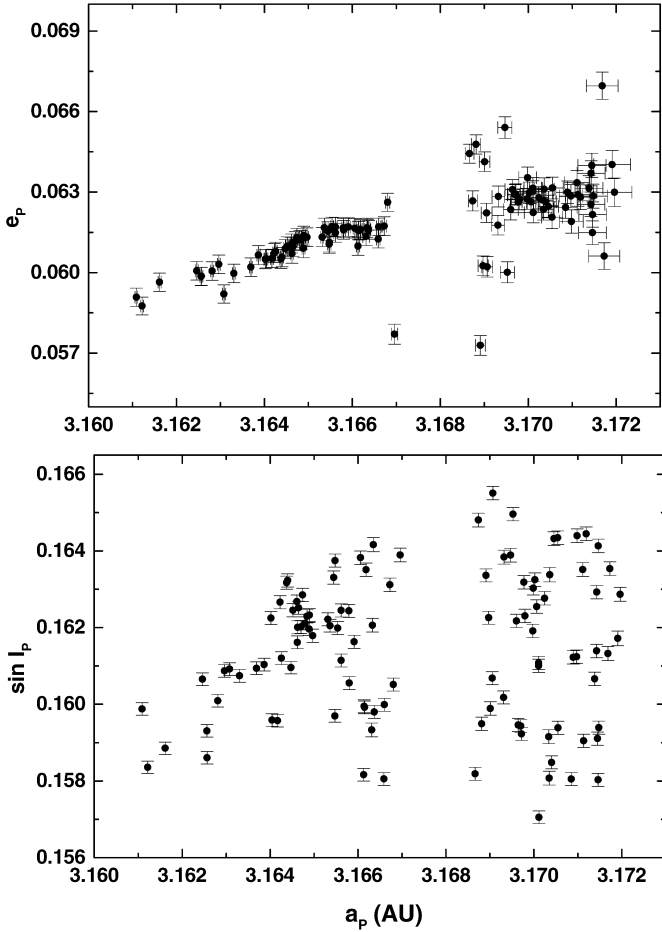


Fig. 5. Evolution of the proper elements of  $R_1$ ,  $R_2$  and non-chaotic group- $B$  family members for 10 Myr. Each dot represents the mean location of a body on the  $(a_p, e_p)$ —top— and  $(a_p, \sin i_p)$ —bottom—plane. Each error-bar has length equal to the standard deviation of the values of the corresponding proper element, as taken from the 10 Myr time series. As shown in the plots, all these bodies have very stable proper elements. The results remained practically the same, when we extended our integration to 100 Myr, for a representative sample of these bodies.

The different evolutionary paths of asteroids in the two main resonances can be better appreciated by looking at Fig. 7. The traces of the 10 Myr evolution of two group- $A$  asteroids (dark-grey and light-grey dots) and three group- $B$  asteroids (black, dark-grey, and light-grey dots) are superimposed on the present-day  $(a_p, e_p)$  distribution of the Veritas family members (triangles). It is clear from the plot that group- $A$  asteroids span the same phase-space region, while each of the three group- $B$  bodies follows its own path in phase space. This result also shows that most  $(5, -2, -2)$  harmonics overlap efficiently, creating a single chaotic zone in which all bodies diffuse. On the contrary, the  $(3, 3, -2)$  harmonics are probably marginally overlapping, for such small values of  $e_p$ . As a result, each asteroid follows, most of the time, ‘its own’  $(3, 3, -2)$  harmonic, while being perturbed by neighboring resonances of the same multiplet. We found several chaotic group- $B$  bodies, whose mean semi-major axis performs small ‘jumps’—from one component of the resonance multiplet to another—on a 100 Myr time interval.

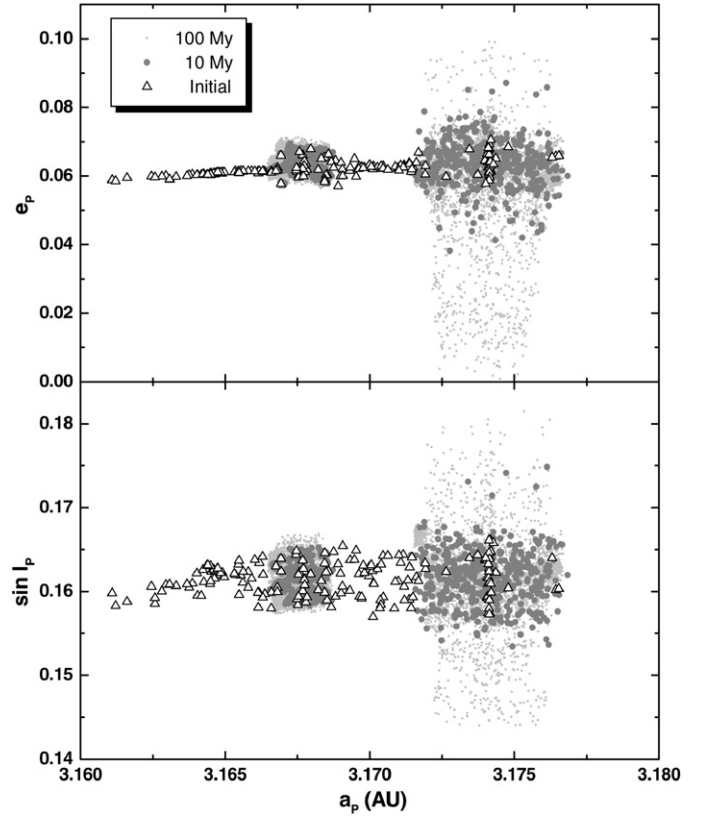


Fig. 6. Dynamical evolution of the members of the two chaotic groups in the space of proper elements:  $(a_p, e_p)$  on the top and  $(a_p, \sin i_p)$  at the bottom. The triangles denote the positions of the family members at present. Dark-grey dots are the traces of the bodies of the two chaotic groups, within 10 Myr of evolution. Light-grey small dots are the traces of the same bodies after a 100 Myr of evolution. The superposition clearly shows that group- $A$  bodies diffuse significantly already over a 10 Myr time scale. Conversely, for group- $B$  bodies, no diffusion is observed over a 100 Myr time interval.

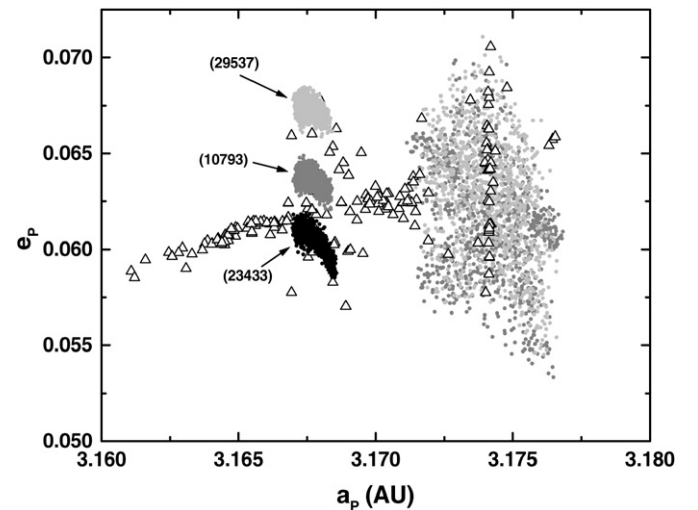


Fig. 7. Dynamical evolution of two group- $A$  and three group- $B$  bodies in  $(a_p, e_p)$  space for 10 Myr. As shown in the plot, group- $A$  bodies span the same phase-space region. This is not true for group- $B$  bodies, each of which seems to occupy ‘its own’ resonance zone.

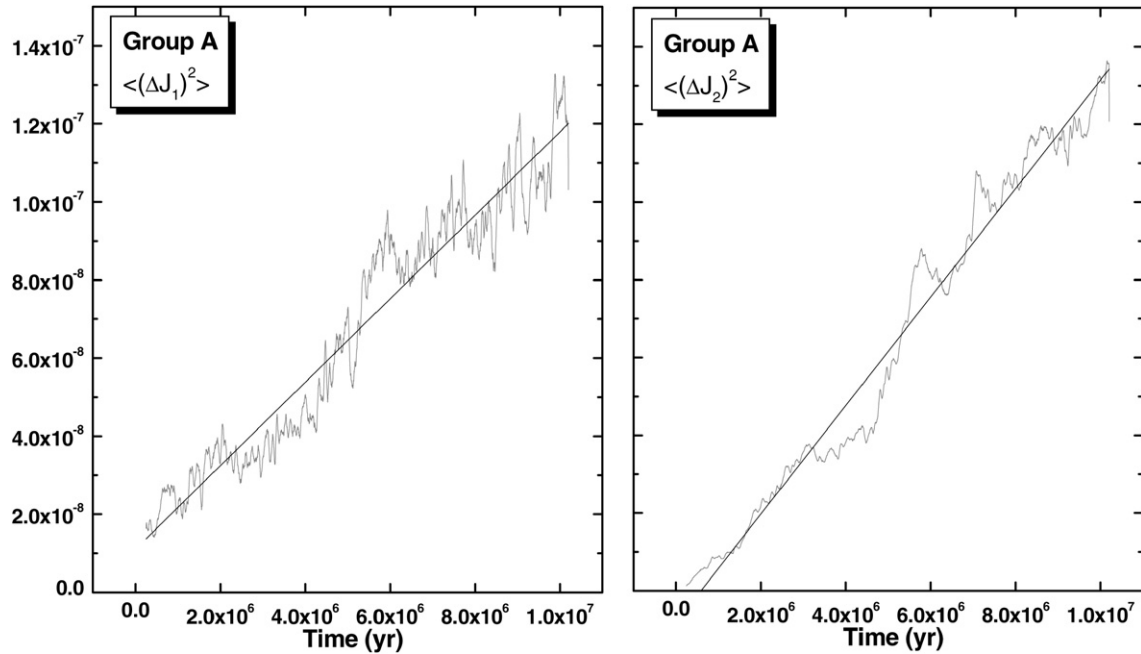


Fig. 8. The mean squared displacement in  $J_1$  (left) and  $J_2$  (right) as a function of time, for group-A bodies. The scale is the same in both panels. The grey curves are the data. The black straight lines are the results of a least-squares fit. Their slopes define the corresponding diffusion coefficients.

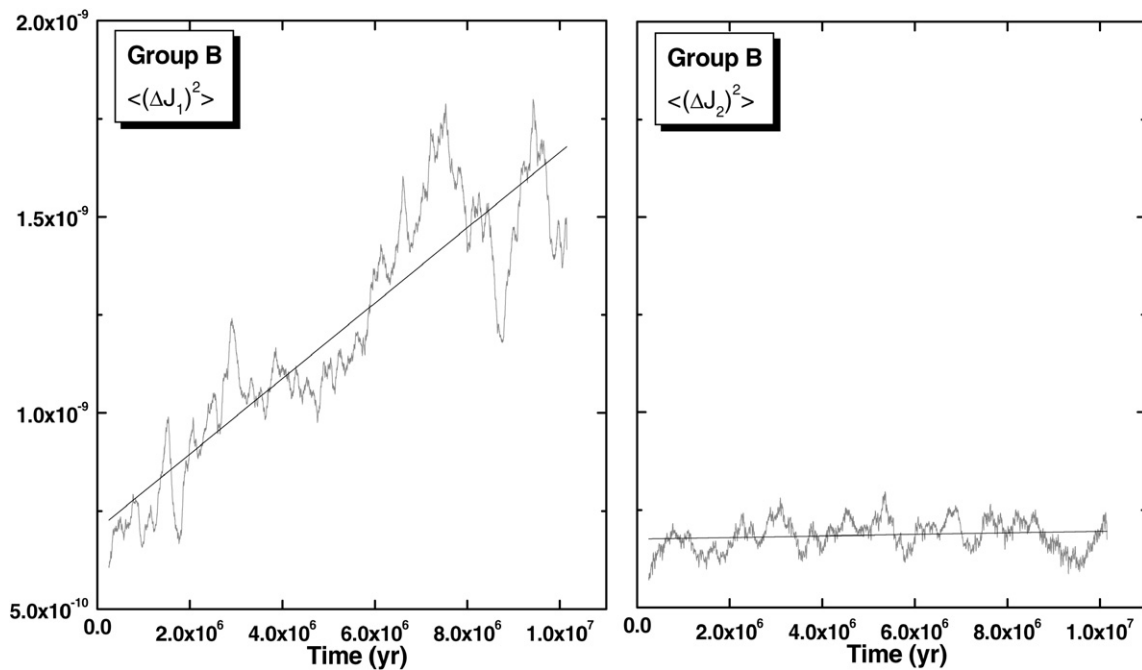


Fig. 9. The same as Fig. 8, but for group-B bodies.  $\mathcal{D}(J_1)$  is much smaller than for group-A bodies, while  $\mathcal{D}(J_2)$  is almost zero (the scale is the same in both panels, but different from Fig. 8).

However, this type of chaotic motion does not seem to produce significant macroscopic diffusion in  $e_p$  and  $\sin i_p$ .

Using our 10 Myr integration of the real bodies, we computed the diffusion coefficients in  $J_1$  and  $J_2$ , as explained in Section 2, for both chaotic groups. The results are shown in Figs. 8 and 9. For group-A asteroids (Fig. 8), the mean squared displacement in both actions is clearly a linear function of time. The corresponding values of the diffusion coefficient are of similar magnitude,  $\mathcal{D}(J_1) = (1.07 \pm 0.02) \times 10^{-14} \text{ yr}^{-1}$  and

$\mathcal{D}(J_2) = (1.39 \pm 0.02) \times 10^{-14} \text{ yr}^{-1}$ . The uncertainties given here represent 67% confidence intervals (or  $1 - \sigma$  intervals) for the slope of the least-squares line. In what follows we will use similar confidence intervals in all statistical estimates. For the chaotic group-B asteroids, we found a much smaller value for  $\mathcal{D}(J_1) = (9.60 \pm 0.13) \times 10^{-17} \text{ yr}^{-1}$  and a practically zero value for  $\mathcal{D}(J_2) = (1.89 \pm 0.03) \times 10^{-18} \text{ yr}^{-1}$ . Thus, chaotic motion is strongly diffusive for group A, while it is almost non-diffusive for group B. In fact, our results for group B show that

motion in this region effectively takes place on a 2-D surface of nearly-constant  $J_2$  in the 3-D action space. In such a 2-D model, the near-conservation of an averaged resonant Hamiltonian would practically restrict diffusion within thin layers, formed around a guiding curve in  $(a, e)$  space (see Fig. 7), which is characteristic of the path of a resonant asteroid in the single-resonance integrable approximation (see Morbidelli, 2002; Tsiganis and Morbidelli, 2003).

### 3.4. Chaotic chronology and the age of the family

We integrated backwards in time the orbits of the 50 family members of  $R_1$  for 10 Myr and calculated their proper elements time series. Following Nesvorný et al. (2003), we calculated the mean difference of nodal longitudes of all bodies,  $\langle \Delta \Omega \rangle$ , with respect to (1086) Nata as a function of time (Fig. 10). A clustering of the nodes within  $30^\circ$  was found at  $t = -8.3$  Myr. When we extended the simulation to  $t = -100$  Myr (the upper bound for the age of the family) we did not observe any other clustering. This result not only confirms the 8.3 Myr age estimate of Nesvorný et al. (2003), but also supports their statistical arguments against multiple random clusterings. Our results show a more tight clustering of the nodes [within  $30^\circ$ , instead of  $41^\circ$  found by Nesvorný et al. (2003)] mainly because (i) we excluded from the calculation all non-chaotic group- $B$  and  $R_2$  family members, whose proper nodal frequencies are modulated by the nearby resonances, and (ii) we performed the calculation using proper elements, thus reducing the effects of high-frequency variations.

A comment should be made here, concerning the action of the Yarkovsky thermal force, which is neglected in the present analysis. As discussed in Section 3, the Yarkovsky-induced radial migration of Veritas family members can be ignored, since it amounts to a very small change in  $a$ , compared to the extent of the family. However, a small change in  $a$  can result to non-negligible changes of the secular frequencies,  $\dot{\omega}$  and  $\dot{\Omega}$ , thus reducing the accuracy of the age estimate, as derived from the

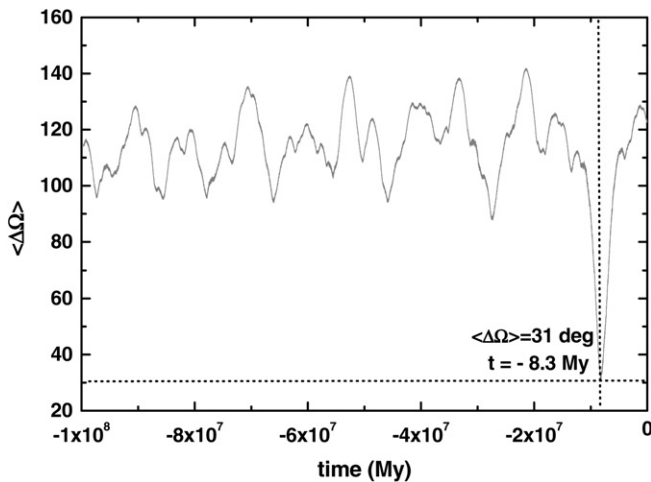


Fig. 10. The mean difference in nodal longitude of  $R_1$  bodies, with respect to (1086) Nata, as a function of time. A nodal conjunction within  $31^\circ$  is observed for  $t = -8.3$  Myr. No other clustering can be seen, within a 100 Myr time interval.

angles-clustering method. Correcting for this effect, Nesvorný and Bottke (2004) were able to calculate the age of the Karin cluster with a 0.05 Myr accuracy and estimate the thermal conductivity of its members. For the Veritas family, the change in the secular frequencies is even larger than in the Karin region, due to the proximity of the 2:1 mean motion resonance (at  $\sim 3.3$  AU; see also Milani and Knežević, 1994). As was noted in Nesvorný et al. (2003), this is most likely the reason for which no clear clustering of the pericenters can be seen in the past integration of the  $R_1$  group.

An independent estimate of the age of the family can be obtained, by applying a modified chaotic chronology method in group A. As shown in the previous section, the members of this group have a diffusive evolution in  $e_P$  and  $i_P$ . Let us assume that the diffusion coefficients are constant throughout the range of  $e_P$  and  $i_P$  spanned by these objects. Then, a simple random-walk model can be used to describe their evolution, where, during a time interval  $\Delta t$ , each body undergoes a random ‘jump’ in  $J_1$  and  $J_2$ , of a length given by a 2-D Gaussian distribution. The values of  $\mathcal{D}(J_1)$  and  $\mathcal{D}(J_2)$  correspond to the standard deviation of the projections of the probability density, along the  $J_1$  and  $J_2$  axis, respectively.

Four snapshots of the evolution of a fictitious initial distribution of 400 (5, -2, -2)-resonant bodies in the  $(e_P, \sin i_P)$  space, according to our random-walk model, are shown in Fig. 11. The initial distribution is assumed to be as extended as suggested by the equivelocity ellipses drawn in Fig. 1. The area of the plane covered by the real group-A members, when the latter are propagated for 10 Myr into the future (Run II), is also shown (grey dots). The box plotted in all panels indicates the size of the present-day distribution of group-A family members. The fictitious objects are spreading diffusively in action space, the variance of the distribution growing linearly with time. The box is filled by our random-walkers within less than 10 Myr. Note that although several particles have leaked out of the box at  $t = 10$  Myr, the standard deviation in both variables is still smaller than the corresponding side of the box, i.e., more than 67% of the particles is well contained within the box. The dimensions of the 2-D distribution of random-walkers at  $t = 10$  Myr, as given by the mean value plus/minus the standard deviation of each proper element, are  $\langle e_P \rangle \pm \sigma(e_P) = 0.064 \pm 0.005$  and  $\langle \sin i_P \rangle \pm \sigma(\sin i_P) = 0.162 \pm 0.002$ . At  $t = 20$  Myr, the random-walkers cover an area, which has approximately the same extent as the one covered by the future images of real group-A members (the results of Run II). The above results confirm that a simple random-walk approach can be used to obtain an estimate for the age of group A. In fact Fig. 11 already indicates that the age of this group must be  $\sim 10$  Myr.

Of course, as shown in Fig. 11, the diffusion zone spanned by group-A asteroids does not have the simple elliptical shape of the region covered by the random-walkers. In particular it has three ‘tails,’ two at small and one at high eccentricities, while most of the bodies seem to occupy a more compact region. This suggests that, as the resonant bodies spread, they approach phase-space regions, characterized by different transport properties: the diffusion coefficient may vary significantly, with respect to the region occupied by the present-day distrib-

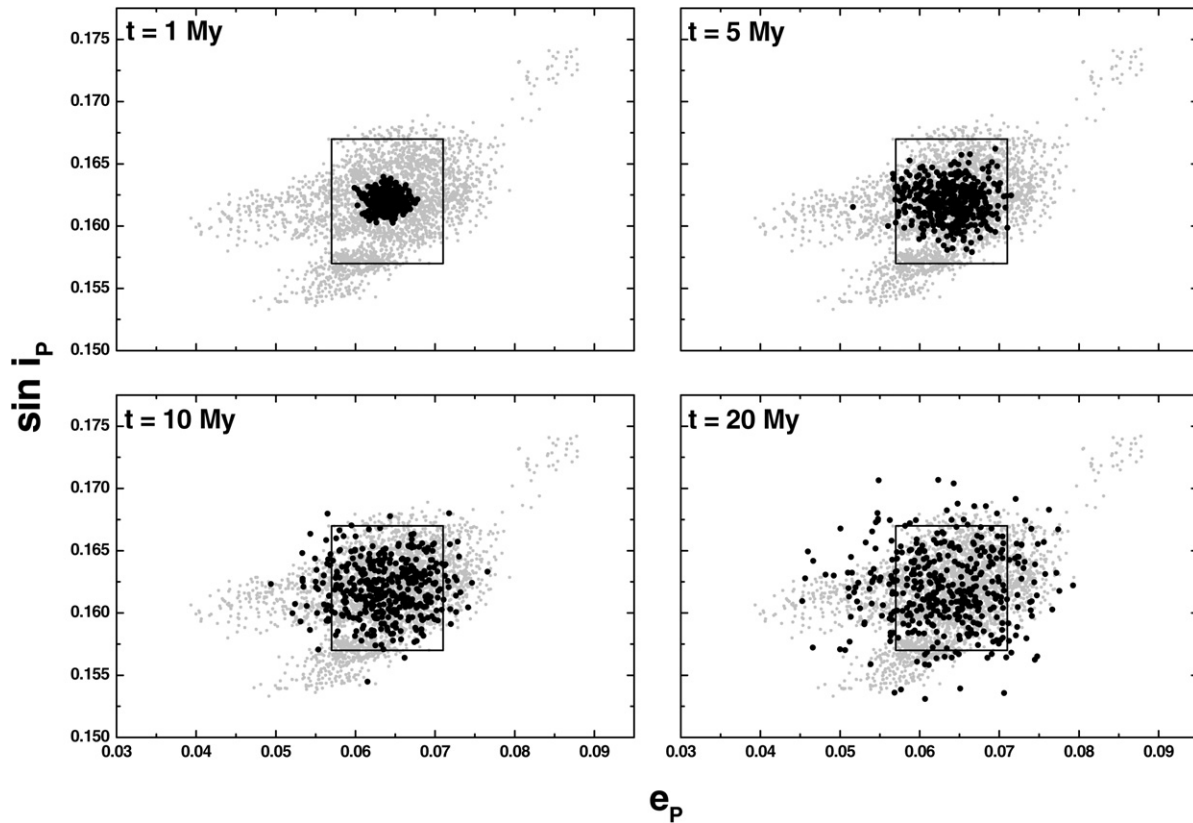


Fig. 11. Evolution of a set of 400 fictitious asteroids (black dots), according to our random-walk model. The values of the diffusion coefficients are the ones derived for the  $(5, -2, -2)$  region. The four snapshots correspond to 1 Myr (top-left), 5 Myr (top-right), 10 Myr (bottom-left) and 20 Myr (bottom-right) of evolution. The grey dots are the traces of the real resonant family members, propagated for 10 Myr, and represent the extent of the diffusion zone. As shown in the plots, it takes less than 10 Myr for the random-walkers to fill the region occupied by the present-day distribution of the real  $(5, -2, -2)$  Veritas family members (box), and  $\sim 20$  Myr to cover the same area as the future images of the real objects.

ution of group-*A* bodies, or transport may deviate significantly from normal diffusion, due to a complex phase-space topology. In either case, what the above results show is that normal diffusion is only an approximation of the real transport process. A more advanced Monte Carlo technique could be used, in which the diffusion region would be split into a number of cells, each one being assigned different values for  $\mathcal{D}$ . However, for what concerns the purpose of the present study, we are satisfied with the fact that the simplest approximation seems to provide a good estimate for the transport time scale. We reserve the analysis of a more refined computational method for future work.

Before performing a refined estimate for the age of group *A*, let us review the simple case of 1-D normal diffusion. The solution of the 1-D diffusion equation

$$\frac{\partial f(x, t)}{\partial t} = \frac{\partial}{\partial x} \left( \frac{\mathcal{D}(x)}{2} \frac{\partial f(x, t)}{\partial x} \right) \quad (1)$$

for a constant coefficient  $\mathcal{D}(x) = \mathcal{D}$  and for  $f(x_0, t = 0) = \delta(x_0)$  is a Gaussian distribution, whose variance is a linear function of time

$$\sigma^2(x) = \frac{\mathcal{D}}{2} t. \quad (2)$$

The above equation is also known as Fick's law. In Eq. (1),  $f$  denotes the probability density and  $x$  a generic action variable. We note that Eq. (1) is the Fokker–Planck transport equa-

tion, written in a form particular to Hamiltonian systems (hence the factor of 1/2 appearing in the r.h.s.; see [Lichtenberg and Lieberman, 1983](#)). Using the value of  $\mathcal{D}(J_1)$  obtained before and the value of  $\sigma(J_1) = (2.19 \pm 0.16) \times 10^{-4}$  calculated from the distribution of the real group-*A* members, we estimate the age of group *A* to be  $\tau_1 = (9.0 \pm 1.3)$  Myr. The error in  $\sigma(J_1)$  corresponds to the length of the 67% confidence interval and the typical error in  $\tau$  is computed by expanding Eq. (2) to first order in the small quantities. A similar calculation can be performed for the  $J_2$  distribution. The corresponding values are  $\sigma(J_2) = (3.61 \pm 0.26) \times 10^{-4}$  and  $\tau_2 = (18.6 \pm 2.7)$  Myr. The discrepancy between  $\tau_1$  and  $\tau_2$  shows that the 1-D approach is not sufficient to obtain an accurate age estimate for group *A*, as  $\tau_1$  is statistically compatible with the 8.3 Myr estimate for the regular component of the family, while  $\tau_2$  is twice as large. However, we note that  $\tau_1$  must be closer to the “true” age, since Eq. (2) requires that the distribution of family members immediately after break-up resembled closely a delta function. The equivelocity curves plotted in [Fig. 1](#) suggest that the initial  $J_1$  distribution was satisfying the above condition much better than the one of  $J_2$ .

In order to obtain an accurate age estimate for group *A*, a 2-D diffusion model has to be employed. We make use of the random-walk model, presented in the previous paragraph, which is equivalent to solving the discretized 2-D Fokker–

Planck equation. In each run we use 2000 fictitious asteroids, initially distributed randomly in a region of size  $\delta J_1(0)$  and  $\delta J_2(0)$ . We define the age of the group,  $\tau$ , as the time needed for the distribution of random-walkers to reach the borders of the present-day distribution, i.e., we stop the integration when 0.3% of the particles are  $\pm 3\sigma(J_i)$  ( $i = 1, 2$ ) away from the origin. In order to be able to calculate a  $1 - \sigma$  confidence interval for  $\tau$ , we perform 100 different runs with the same values of  $\delta J_1(0)$  and  $\delta J_2(0)$  but with  $\mathcal{D}(J_i)$  and  $\sigma(J_i)$  randomly selected, each from a Gaussian distribution, whose mean value and standard deviation are equal to the central value and half-width of the corresponding confidence interval.

For  $\delta J_1(0) = 1.2 \times 10^{-4}$  and  $\delta J_2(0) = 5.6 \times 10^{-4}$ , which are the values suggested by the equivelocity ellipses shown in Fig. 1, we find

$$\tau = \langle \tau \rangle \pm \sigma(\tau) = (8.7 \pm 1.7) \text{ Myr}. \quad (3)$$

The distribution of  $\tau$ 's for this experiment is shown in Fig. 12 (top). In order to examine the dependence of  $\tau$  on the initial size of the family, the above calculations were repeated for five different values of  $\delta J_1(0)$  (in the range  $[0.2 \times 10^{-4}, 2.3 \times 10^{-4}]$ ) and three different values of  $\delta J_2(0)$ , (in the range  $[2.7 \times 10^{-4}, 11.2 \times 10^{-4}]$ ). As shown in Fig. 12 (bottom),  $\tau$  is roughly independent of the initial size of the distribution for variations within a factor of four, the corresponding range

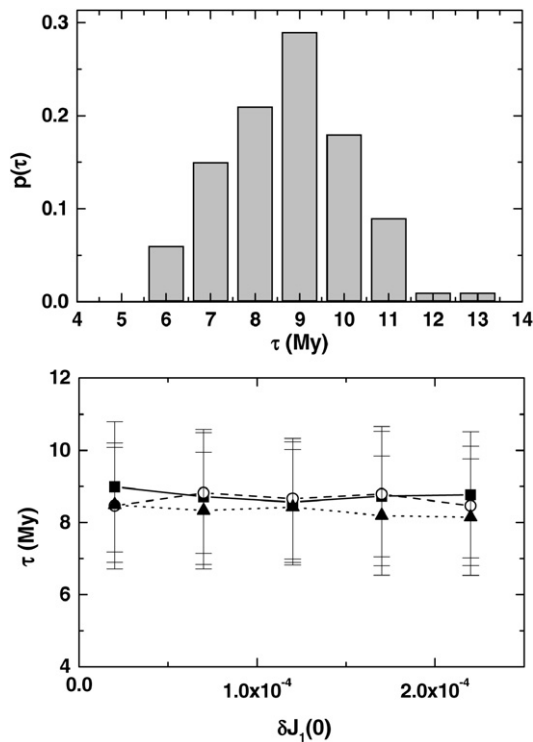


Fig. 12. (Top) Histogram of  $\tau$ -values, for the diffusive group *A* of the Veritas family. The distribution was produced by performing 100 runs of the random-walk model, each using 2000 fictitious group-*A* members. The initial spread in both actions was the same for all trials. The age is found to be  $\tau = (8.7 \pm 1.7)$  Myr. (Bottom) Dependence of  $\langle \tau \rangle$  and  $\sigma(\tau)$  on  $\delta J_1(0)$ . Three different sets of symbols are shown, representing three different values of  $\delta J_2(0)$  (see text). As seen in the figure, for moderate changes in the initial values of  $\delta J_1$  and  $\delta J_2$ , both  $\langle \tau \rangle$  and  $\sigma(\tau)$  remain practically unchanged.

of  $\tau$  values being  $7.9 \leq \langle \tau \rangle \leq 9.0$  and  $1.6 \leq \sigma(\tau) \leq 1.9$ . These results show that the 1-D model of eccentricity diffusion indeed gives a good estimate for  $\tau$ . The fact that the corresponding 1-D equation for inclination diffusion gives  $\tau_2 \sim 2\tau$  further suggests that much of the observed spread in  $J_2$  ( $\sim 70\%$ ) is most probably due to a large vertical component of the ejection velocity field.

According to the results presented in this section, both  $R_1$  and the chaotic group *A* have the same age, within the statistical uncertainties. However, the large spread of group *B* still seems puzzling. The diffusion coefficient for this group is  $\sim 100$  times smaller than for group *A*. At this rate, group-*B* bodies would need  $\sim 300$  Myr to cover their observed size in  $e_p$ . If the Veritas family was that old, group-*A* bodies would have diffused away from the family region and the distribution of asteroids at  $a_p \approx 3.174$  AU would be practically flat in  $e_p$  and  $\sin i_p$ . It is easy to check that this is not true and that the number of Veritas family members in each group is  $\sim 8$  times larger than the number of background asteroids. Besides, both the chaotic and the non-chaotic part of group *B* have similar extent in  $e_p$  (0.010 and 0.008, respectively), while the variations of  $e_p$  over 10 Myr are also of similar magnitude (0.007 and 0.006) and amount to about half the observed spread. These results suggest that either (i) some group-*B* bodies close to the borders of the family are interlopers and the extent of group *B* is actually smaller, or (ii) the observed spread is due to the ejection velocity field and the equivelocity ellipses drawn in Fig. 1 are misleading (i.e., too narrow;  $\Delta e_p = 0.003$  at  $a_p \approx 3.168$  AU). If the first is true, we can expect some interlopers near the borders of group *A* as well. Our estimate of the age would then be somehow smaller than 8.7 Myr but not much, since the distribution of group-*A* bodies in  $J_1$  is close to a Gaussian and thus removing the ‘tails’ would not change significantly the value of  $\sigma(J_i)$ . On the other hand, if the observed extent of group *B* is real, we have to assume an equivelocity curve twice as wide in  $e_p$ . This corresponds to increasing  $\delta J_1(0)$  by a factor of four, with respect to our ‘nominal’ run. However, even for this value of  $\delta J_1(0)$ , our random-walk model gives  $\tau = (7.9 \pm 1.7)$  Myr.

#### 4. Conclusions

In this paper we analyzed the dynamical evolution of the Veritas family, as a typical example of a young and dynamically complex asteroid family. The analysis presented here could be applied to other dynamically heterogeneous families. For extended families that are much older than 10 Myr, the crossing of different high-order resonances by small family members (due to the Yarkovsky effect) should be taken into account. On the other hand, if the family comprises an adequate number of large bodies ( $D > 20$  km), for which the Yarkovsky effect can be ignored, the present analysis could be restricted to that subgroup only.

The method of chaotic chronology is probably better suited for old asteroid families, since the effects of chaotic diffusion

can be better calibrated on time scales longer than 100 Myr.<sup>7</sup> Previous studies have made use of long-term numerical integrations of family members (also including the Yarkovsky effect), in order to assess the effects of chaos on the shape of asteroid families and derive upper or lower bounds for their ages (see Nesvorný et al., 2002c; also Carruba et al., 2005). The method presented here follows a different path; it is based on a statistical description of asteroid transport. The critical parameters are the diffusion coefficients, which are calculated using relatively short numerical integrations (a few Myrs). It is possible to further refine our random-walk model, by calculating the coefficient of chaotic diffusion at different locations within the family, and also include the variations of  $a_p$  of family members due to the Yarkovsky effect. Such a procedure would provide an accurate statistical modeling of the combined action of the Yarkovsky drift and chaotic diffusion.

Different resonances are responsible for different types of chaotic motion within the Veritas family: stable chaos, on one hand, and diffusive chaos, on the other. The most important chaotic group is composed of bodies that reside in the (5, -2, -2) three-body resonance, including (490) Veritas itself. As the evolution in this resonance is diffusive, this group of bodies can be used to accurately estimate the age of the family. By measuring the diffusion rate of these objects in proper elements space, and assuming transport to be well approximated by normal 2-D diffusion, we were able to derive an age estimate of  $\tau = 8.7 \pm 1.7$  Myr. The error in  $\tau$  is mainly due to the errors in estimating  $\mathcal{D}(J_i)$  and  $\sigma(J_i)$ , both of which depend on the size of the sample.

Our estimate for the age of the Veritas family is statistically indistinguishable from the one of 8.3 Myr, derived by Nesvorný et al. (2003). Our application of the Nesvorný et al. (2002a) method also corroborated the above result, revealing a unique nodal conjunction at  $t = -8.3$  Myr within a 100 Myr integration time span. Nesvorný et al. (2003) discussed the possibility that the 8.3 Myr age estimate corresponds to a secondary break-up within the Veritas family, responsible for the formation of the  $R_1$  group (in our notation). Our results on the chaotic component of the family suggest that both the (1086) Nata group of regular bodies and the (490) Veritas group of chaotic bodies were formed at the same time. This conclusion is in agreement with those of Farley et al. (2006), whose analysis showed that the break-up of a single large ( $\sim 150$  km) asteroid  $\sim 8.3$  Myr ago (assumed to be the progenitor of the whole Veritas family) can explain the corresponding  $^3\text{He}$  peak, observed in sea-floor dust sedimentation records.

Our analysis was based on a sample of 180 family members. Although the statistics could be improved by using an updated catalogue of numbered and multi-opposition bodies, our results would not change significantly. The dynamical groups would be still the same and the variance in  $e_p$  and  $\sin i_p$  would be similar.

The chronology method of Nesvorný et al. (2002a) is quite efficient. However, it cannot be readily applied in regions of the asteroid belt where chaotic diffusion is prominent. Hence, when

studying dynamically heterogeneous families, complementary information should be obtained, by applying both the method of Nesvorný et al. (2002a) on the regular component of the family and our revised chaotic chronology method on the chaotic component. Of course the chaotic chronology method is not as accurate as the one of Nesvorný et al. (2002a), as it is based on an approximate description of the transport process, for an ensemble of chaotic bodies. Even so, it adequately describes the spreading of diffusive family members in the space of proper elements. As shown in Nesvorný et al. (2003), several small asteroid clusters, probably representing recent asteroid break-ups, exist in regions of the main belt where chaotic diffusion is strong. Such asteroid groupings could be approximately dated, using the method presented in this paper.

### Acknowledgments

We thank Andrea Milani, David Nesvorný and Alessandro Morbidelli for their critical reading of the first version of the manuscript and for their useful comments and suggestions, which greatly improved the presentation of our work. This research has been partly funded by the Ministry of Science and Environmental Protection of Serbia (project 146004) “Dynamics of Celestial Bodies, Systems and Populations” and by the EPEAEK II/Pythagoras I programme of the Greek Ministry of Education.

### References

- Botke, W.F., Vokrouhlický, D., Broz, M., Nesvorný, D., Morbidelli, A., 2001. Dynamical spreading of asteroid families via the Yarkovsky effect. *Science* 294, 1693–1696.
- Carruba, V., Michtchenko, T.A., Roig, F., Ferraz-Mello, S., Nesvorný, D., 2005. On the V-type asteroids outside the Vesta family. I. Interplay of nonlinear secular resonances and the Yarkovsky effect: The cases of 956 Elisa and 809 Lunda. *Astron. Astrophys.* 441, 819–829.
- Dermott, S.F., Kehoe, T.J.J., Durda, D.D., Grogan, K., Nesvorný, D., 2002. Recent rubble-pile origin of asteroidal Solar System dust bands and asteroidal interplanetary dust particles. In: Warmbein, B. (Ed.), *Proceedings of Asteroids, Comets, Meteors. (ACM 2002)*. In: ESASP-500. ESA, Noordwijk, pp. 319–322.
- Di Martino, M., Migliorini, F., Zappalà, V., Manara, A., Barbieri, C., 1997. Veritas asteroid family: Remarkable spectral differences inside a primitive parent body. *Icarus* 127, 112–120.
- Farinella, P., Vokrouhlický, D., 1999. Semi-major axis mobility of asteroid fragments. *Science* 283, 1507–1510.
- Farley, K.A., Vokrouhlický, D., Bottke, W.F., Nesvorný, D., 2006. A late Miocene dust shower from the break-up of an asteroid in the main belt. *Nature* 439, 295–297.
- Hirayama, K., 1918. Groups of asteroids probably of common origin. *Astron. J.* 31, 185–188.
- Knežević, Z., 1999. Veritas family age revisited. In: Svoren, J., Pittich, E.M., Rickman, H. (Eds.), *Evolution and Source Regions of Asteroids and Comets*. In: *Proceedings of IAU Colloquium*, vol. 173. *Astron. Inst. Slovak Acad. Sci., Tatranska Lomnica*, pp. 153–158.
- Knežević, Z., Pavlović, R., 2002. Young age for the Veritas asteroid family confirmed? *Earth Moon Planets* 88, 155–166.
- Knežević, Z., Tsiganis, K., Varvoglis, H., 2002. Dynamical portrait of the Veritas family region. In: Warmbein, B. (Ed.), *Proceedings of Asteroids, Comets, Meteors. (ACM 2002)*. In: ESA SP-500. ESA, Noordwijk, pp. 335–338.
- Lichtenberg, A.J., Leiberman, M.A., 1983. *Regular and Stochastic Motion*. Springer-Verlag, New York.

<sup>7</sup> Although the complexity of a larger phase-space region would certainly produce problems in the statistical analysis.

- Milani, A., Farinella, P., 1994. The age of the Veritas asteroid family deduced by chaotic chronology. *Nature* 370, 40–42.
- Milani, A., Knežević, Z., 1994. Asteroid proper elements and the dynamical structure of the main belt. *Icarus* 107, 219–254.
- Milani, A., Nobili, A.M., 1992. An example of stable chaos in the Solar System. *Nature* 357, 569–571.
- Morbidelli, A., 2002. *Modern Celestial Mechanics: Aspects of Solar System Dynamics*. Taylor & Francis, London.
- Morbidelli, A., Zappalà, V., Moons, M., Cellino, A., Gonczi, R., 1995. Asteroid families close to mean motion resonances: Dynamical effects and physical implications. *Icarus* 118, 132–154.
- Murray, N., Holman, M., 1997. Diffusive chaos in the outer belt. *Astron. J.* 114, 1246–1259.
- Nesvorný, D., Bottke, W.F., 2004. Detection of the Yarkovsky effect for main-belt asteroids. *Icarus* 170, 324–342.
- Nesvorný, D., Morbidelli, A., 1998. Three-body mean motion resonances and the chaotic structure of the asteroid belt. *Astron. J.* 116, 3029–3037.
- Nesvorný, D., Morbidelli, A., 1999. An analytic model of three-body mean motion resonances. *Celest. Mech. Dynam. Astron.* 71, 243–271.
- Nesvorný, D., Bottke Jr., W.F., Dones, L., Levison, H.F., 2002a. The recent breakup of an asteroid in the main-belt region. *Nature* 417, 720–722.
- Nesvorný, D., Ferraz-Mello, S., Holman, M., Morbidelli, A., 2002b. Regular and chaotic dynamics in mean-motion resonances: Implications for the structure and evolution of the asteroid belt. In: Bottke, W.F., Cellino, A., Paolicchi, P., Binzel, R.P. (Eds.), *Asteroids III*. Univ. of Arizona Press, Tucson, pp. 379–394.
- Nesvorný, D., Morbidelli, A., Vokrouhlický, D., Bottke, W.F., Brož, M., 2002c. The Flora family: A case of the dynamically dispersed collisional swarm? *Icarus* 157, 155–172.
- Nesvorný, D., Bottke, W.F., Levison, H.F., Dones, L., 2003. Recent origin of the Solar System dust bands. *Astrophys. J.* 591, 486–497.
- Paolicchi, P., Dell’Oro, A., Cellino, A., La Spina, A., Zappalà, V., 2002. Fitting the mass distributions of Koronis family: New ideas and related physical constraints. In: Warmbein, B. (Ed.), *Proceedings of Asteroids, Comets, Meteors*. (ACM 2002). In: ESA SP-500. ESA, Noordwijk, pp. 525–528.
- Tsiganis, K., Morbidelli, A., 2003. Chaotic diffusion of small bodies in the Solar System. *Ann. MCFA* 3, 999–1005.
- Tsiganis, K., Varvoglis, H., Morbidelli, A., 2003. Short-lived asteroids in the 7/3 Kirkwood gap and their relationship to the Koronis and Eos families. *Icarus* 166, 131–140.
- Vokrouhlický, D., Brož, M., Bottke, W.F., Nesvorný, D., Morbidelli, A., 2005. Non-gravitational perturbations and evolution of the asteroid main belt. In: Knežević, Z., Milani, A. (Eds.), *Dynamics of Populations of Planetary Systems*. In: *Proceedings of IAU Colloquium*, vol. 197. Cambridge Univ. Press, Cambridge, UK, pp. 145–156.
- Wyatt, M.C., 2005. The origin and evolution of dust belts. In: Knežević, Z., Milani, A. (Eds.), *Dynamics of Populations of Planetary Systems*. In: *Proceedings of IAU Colloquium*, vol. 197. Cambridge Univ. Press, Cambridge, UK, pp. 383–392.
- Zappalà, V., Bendjoya, Ph., Cellino, A., Farinella, P., Froeschlé, C., 1995. Asteroid families: Search of a 12,487-asteroid sample using two different clustering techniques. *Icarus* 116, 291–314.